HHS Public Access

Author manuscript

ACS Appl Mater Interfaces. Author manuscript; available in PMC 2018 April 26.

Published in final edited form as:

ACS Appl Mater Interfaces. 2017 September 13; 9(36): 30297–30305. doi:10.1021/acsami.7b05654.

Quantum-Dot-Based Theranostic Micelles Conjugated with an Anti-EGFR Nanobody for Triple-Negative Breast Cancer Therapy

Yuyuan Wang[†], **Yidan Wang**[‡], **Guojun Chen**[†], **Yitong Li**[§], **Wei Xu**[‡,*,‖], and **Shaoqin Gong**[†,*,⊥]

[†]Department of Materials Science and Engineering and Wisconsin Institute for Discovery, University of Wisconsin—Madison, 330 N. Orchard Street, Madison, Wisconsin 53715, United States

[‡]McArdle Laboratory for Cancer Research, University of Wisconsin—Madison, 1111 Highland Avenue, Madison, Wisconsin 53706, United States

[§]Department of Chemistry, Tsinghua University, 30 Shuangqing Road, Beijing 100084, China

[‖]Molecular and Environmental Toxicology Center, University of Wisconsin—Madison, 1300 University Avenue, Madison, Wisconsin 53706, United States

[⊥]Department of Biomedical Engineering, University of Wisconsin—Madison, 1550 Engineering Drive, Madison, Wisconsin 53706, United States

Abstract

A quantum-dot (QD)-based micelle conjugated with an anti-epidermal growth factor receptor (EGFR) nanobody (Nb) and loaded with an anticancer drug, aminoflavone (AF), has been engineered for EGFR-overexpressing cancer theranostics. The near-infrared (NIR) fluorescence of the indium phosphate core/zinc sulfide shell QDs (InP/ZnS QDs) allowed for *in vivo* nanoparticle biodistribution studies. The anti-EGFR nanobody 7D12 conjugation improved the cellular uptake and cytotoxicity of the QD-based micelles in EGFR-overexpressing MDA-MB-468 triple-negative breast cancer (TNBC) cells. In comparison with the AF-encapsulated nontargeted (i.e., without Nb conjugation) micelles, the AF-encapsulated Nb-conjugated (i.e., targeted) micelles accumulated in tumors at higher concentrations, leading to more effective tumor regression in an orthotopic triple-negative breast cancer xenograft mouse model. Furthermore, there was no systemic toxicity observed with the treatments. Thus, this QD-based Nb-conjugated micelle may serve as an effective theranostic nanoplatform for EGFR-overexpressing cancers such as TNBCs.

Graphical Abstract

[*]Corresponding Authors: wxu@oncology.wisc.edu. shaoqingong@wisc.edu.

ORCID

Shaoqin Gong: 0000-0001-9447-2938

Notes

The authors declare no competing financial interest.

Supporting Information

The Supporting Information is available free of charge on the ACS Publications website at DOI: 10.1021/acsami.7b05654. TEM images of the InP/ZnS QDs and QD-PLA-PEG micelles, UV–vis absorption and photoluminescence (PL) spectra of QDs, change of nanoparticle size as a function of incubation time in various media, and calculation of the molar mass of QD (PDF)

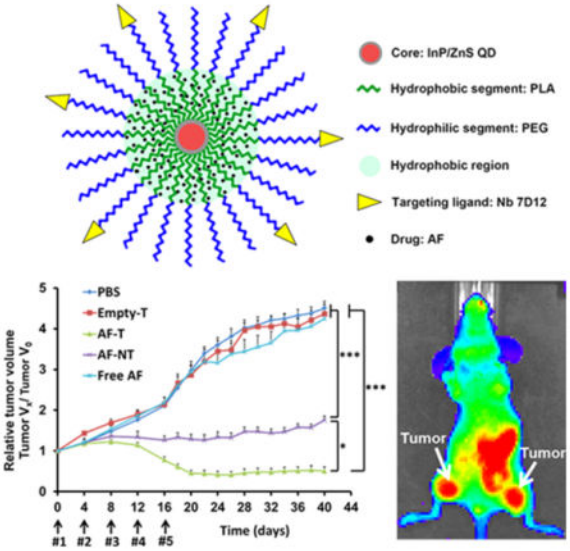

Keywords

quantum dot; nanobody; cancer theranostics; micelle; triple-negative breast cancer

INTRODUCTION

Nanotheranostics, the integration of diagnostic and therapeutic functions into a nanoplatform, enables simultaneous imaging and therapy, thereby making personalized medicine possible. Nanotheranostics is particularly attractive for targeted cancer theranostics because it can achieve passive and receptor-specific active tumor targeting, improve the chemical stability and plasma half-life of the agents, and potentially minimize multidrug resistance.[1–8]

Quantum dots (QDs) with NIR fluorescence are highly desirable for targeted cancer imaging for the following reasons: (1) QDs possess high quantum yields, high molar extinction coefficients, large effective Stokes shifts, high photostability, and tunable emission wavelengths;[9,10] (2) NIR emitted by QDs has deep tissue penetration;[11,12] and (3) QDs can be conveniently functionalized by various molecules.[13,14] As such, QDs have been actively studied and utilized for both *in vitro* and *in vivo* imaging.[9,13–15] An indium phosphate core/zinc acetate shell QD (InP/ZnS QD) was chosen because InP/ZnS QDs are less cytotoxic than other cadmium-based QDs (e.g., cadmium selenide (CdSe) QDs and cadmium sulfide (CdS) QDs).[16–19]

Polymer micelles are nanoparticles formed by the self-assembly of linear amphiphilic block copolymers. Their utility as drug nanocarriers for targeted cancer therapy has been extensively investigated.[20,21] However, multimolecular nano-particles formed by self-assembly (e.g., liposomes, polymer micelles, and polymersomes) often lack sufficient *in vivo* stability. Micelles formed by either single/individual star amphiphilic block copolymers or inorganic nanoparticles functionalized with amphiphilic block copolymers can provide

excellent stability *in vitro* and *in vivo,* narrow size distribution, high drug loading capacity, and versatile surface chemistry.[4,22–26]

Epidermal growth factor receptor (EGFR) is a cell membrane receptor that mediates downstream signaling pathways supporting tumor cell proliferation, metastasis, and tumor angiogenesis.[27–29] Overexpression and/or mutations of EGFR are frequently found in solid tumors[30–33] (e.g., triple-negative breast cancer (TNBC)[34–36]). Therefore, EGFR is a popular molecular target for nanoparticle-based drug delivery. Anti-EGFR nanobodies may serve as an efficient EGFR-targeting ligand for drug delivery nanoparticles. Nanobodies (Nbs) are low molecular weight proteins (~15 kDa) derived from heavy-chain-only antibodies. Antibodies (Abs) and antibody fragments have been extensively explored as tumor-targeting ligands for drug nanocarriers designed for targeted cancer therapy and diagnosis.[37–39] In contrast, the employment of nanobodies as tumor-targeting ligands for nanomedicines is still in its infancy despite its attractive properties, including high specificity and affinity for the target, small size (1/10 of the regular Ab size), excellent stability, aqueous solubility, reversible refolding, and low immunogenic potential (due to the lack of the Fc component as compared to antibodies).[40–50]

Here we report a unique near-infrared (NIR) fluorescent InP/ZnS QD-based theranostic micelle that can target EGFR-overexpressing cancers (e.g., TNBCs). The QDs were functionalized with amphiphilic block copolymer polylactide-*b*-poly(ethylene glycol) (PLA-PEG) resulting in QD-based PLA-PEG micelles. Anti-EGFR nanobodies, 7D12 Nbs, were conjugated onto the surfaces of the nanocarriers as TNBC-targeting ligands. Aminoflavone (AF), a synthetic flavonoid compound,[51] was employed as the anticancer drug. Our results showed that AF-encapsulated, anti-EGFR 7D12 Nb-conjugated, QD-based theranostic micelles effectively led to tumor regression in an orthotopic EGFR-overexpressing TNBC mouse model. This nanocarrier formulation drastically reduced the effective drug dose needed for inhibiting tumor growth, thereby circumventing systemic toxicity.

MATERIALS AND METHODS

Materials

1-Octadecene (ODE) and indium acetate ($In(Ac)_3$) were bought from TCI America. Zinc acetate ($Zn(Ac)_2$), myristic acid (MA), elemental sulfur, tris(trimethylsilyl)phosphine ($(TMS)_3P$), 3-[4,5-dimethylthiazol-2-yl]-2,5-diphenyl tetrazolium bromide (MTT), tris(2-carboxyethyl)phosphine hydrochloride (TCEP), lactic acid (LA), *N,N′*-dimethylformamide (DMF), 4′,6-diamidino-2-phenyl-indole (DAPI), 4-dimethylamino pyridine (DMAP), and bovine plasma were bought from Sigma-Aldrich. Heterobifunctional PEG derivatives (M_w = 5000 Da), HO-PEG-OCH_3, and HO-PEG-Mal from JenKem Technology were used for this study. 1,3-Dicyclohexylcarbo-diimide (DCC) was bought from ACROS. AF (NSC 686288, 4*H*-1-benzopyran-4-one,5-amino-2-(4-amino-3-fluorophenyl)-6,8-difluoro-7-methyl) was acquired from the repository of the Developmental Therapeutics Program (National Cancer Institute (NCI)) at Frederick. The anti-EGFR nanobody (Nb), 7D12, was kindly provided by Prof. Lei Liu's laboratory at Tsinghua University, China. The buffers for refolding Nbs included the following: (1) renaturation buffer A, 10 mM phosphate-buffered saline (PBS) and 8 M urea, pH 7.4; (2) renaturation buffer B, 10 mM PBS and 6 M urea, pH 7.4; (3)

renaturation buffer C, 10 mM PBS and 4 M urea, pH 7.4; (4) renaturation buffer D, 10 mM PBS and 2 M urea, pH 7.4; and (5) renaturation buffer E, 10 mM PBS, pH 7.4.

Synthesis of Indium Myristate ($In(MA)_3$)

$In(MA)_3$ was synthesized as previously reported.[52] Briefly, a mixture of $In(Ac)_3$ (10 mmol, 2.92 g) and myristic acid (40 mmol, 9.12 g) was heated to 140 °C and stirred for 6 h under an argon atmosphere. The product was precipitated in acetone and filtered. The precipitate was then washed three times by acetone and vacuum-dried to yield $In(MA)_3$.

Synthesis of Indium Phosphate Core/Zinc Sulfide Shell QDs (InP/ZnS QDs)

InP/ZnS QDs were synthesized following a published method with a minor modification.[19,52] A mixture of $In(MA)_3$ (0.2 mmol, 192 mg) and 10 mL of ODE was heated to 140 °C for 1 h in a Schlenk flask under vacuum to remove excessive water. Then, $(TMS)_3P$ (0.2 mmol, 50.2 mg) was introduced to the solution. The resulting mixture was heated to 270 °C rapidly and stirred for 15 min under a N_2 atmosphere until the color of the mixture turned dark red. After the reaction mixture was cooled to room temperature, zinc acetate (0.2 mmol, 37 mg) and elemental sulfur (0.2 mmol, 6.4 mg) were added to the solution under a N_2 flow. Subsequently, the mixture was first heated to 60 °C and stirred for 1 h. Then, it was further heated to 300 °C for 30 min to form the ZnS shell. Once it was cooled to room temperature, the mixture was centrifuged (11 000 rpm, 20 °C) for 30 min. The precipitate was redispersed in 20 mL of chloroform. A 1:1 (v/v) mixture of methyl alcohol and acetone (30 mL) was then added into the above solution and stirred for 15 min, followed by centrifugation (11 000 rpm, 20 °C) for 10 min. The resulting InP/ZnS QDs pellets were collected and vacuum-dried. The molar mass of the QD (M_{QD}) was estimated in the Supporting Information.

Synthesis of Carboxylated InP/ZnS QDs (QD-COOH)

First, the InP/ZnS QDs (15 mg) were dispersed in mercaptoacetic acid (MAA, 10 mL). The mixture was stirred vigorously at room temperature for 72 h. Thereafter, chloroform (5 mL) was added to the mixture, which was subsequently centrifuged (11 000 rpm, 20 °C) for 30 min. The pellets were collected and washed at least three times with chloroform (5 mL), and vacuum-dried at 45 °C to yield the QD-COOH nanoparticles.

Synthesis of Amphiphilic Block Copolymers PLA-PEG-Mal and PLA-PEG-OCH_3

PLA-PEG-Mal was synthesized by ring-opening polymerization of LA using $Sn(Oct)_2$ as the catalyst and Mal-PEG-OH as the macroinitiator. Mal-PEG-OH (0.056 mmol, 280 mg) stored in a 50 mL two-neck flask was heated to 120 °C in an oil bath under a N_2 atmosphere. LA (1.4 mmol, 202 mg) was then slowly introduced into the flask. After the solids melted, a catalytic amount ([catalyst]/[monomer] = 1:1000) of $Sn(Oct)_2$ (1.4 μmol, 0.45 μL) was added and stirred for 24 h under a N_2 atmosphere and precipitated three times using cold diethyl ether. The precipitate was then dried to yield the PLA-PEG-Mal polymer. PLA-PEG-OCH_3 was synthesized similarly using CH_3O-PEG-OH as the macroinitiator. Their chemical structures were conflrmed by proton nuclear magnetic resonance (^{1}HNMR) (Bruker Advance 400, 400 MHz). PLA-PEG-OCH_3 (400 MHz, $CDCl_3$): 5.00–5.45 (16 H, m

COC*H*CH_3), 4.60 (1 H, s, terminal COC*H*CH_3), 3.40–3.50 (450 H, m, OCH_2CH_2 from PEG), 1.30–1.45 (49 H, m, COCHCH_3), and 1.23 (3 H, s, terminal COCHCH_3). PLA-PEG-Mal (400 MHz, $CDCl_3$): 6.55 (2 H, d, Mal), 5.00–5.45 (16 H, m COC*H*CH_3), 4.60 (1 H, s, terminal COC*H*CH_3), 3.40–3.50 (437 H, m, OCH_2CH_2 from PEG), 1.30–1.45 (50 H, m, COCHCH_3), and 1.23 (3 H, s, terminal COCHCH_3).

Synthesis of QD-PLA-PEG-OCH_3/Mal

QD-COOH nanoparticles (0.1 μmol, 9.0 mg) were flrst dispersed in 5 mL of DMF followed by the addition of DCC (10 μmol, 2.1 mg) and DMAP (10 μmol, 1.22 mg) under stirring for 1 h. Thereafter, PLA-PEG-OCH_3 (9 μmol, 56 mg) and PLA-PEG-Mal (1 μmol, 6.22 mg) were introduced and stirred for 24 h. The product was purifled by dialysis against deionized (DI) water (molecular weight cutoff (MWCO): 15 kDa) for 8 h. After lyophilization, the QD-PLA-PEG-OCH_3/Mal nanoparticles were redispersed in 10 mM PBS (pH = 7.4) for 7D12 Nb conjugation. The molar mass of QD-PLA-PEG-OCH_3/Mal was estimated using eq 1.

$$M_{\text{QD-PLA-PEG-OCH}_3\text{/Mal}} = M_{\text{QD}} + 10\text{MW}_{\text{PLA-PEG-Mal}} + 90\text{MW}_{\text{PLA-PEG-OCH}_3} \quad (1)$$

Refolding of 7D12 Nbs

The freeze-dried 7D12 Nb powder was first dissolved into renaturation buffer A. The solution was enclosed in a dialysis bag (MWCO 8 kDa) and dialyzed against renaturation buffers B, C, D, and E (twice) at 4 °C. Renaturation buffer solution (2 L) was used for each dialysis step, and the dialysis media were replaced every 6 h. During dialysis, the dialysis renaturation buffers were continuously stirred. The renatured Nb-containing solution was centrifuged (12 000 g, 4 °C) for 30 min to eliminate remaining impurities or the aggregates formed by misfolded proteins. The supernatant was collected and stored at −80 °C for future use.

Preparation of AF-Encapsulated Micelles

AF-encapsulated micelles were prepared by first dispersing AF (5 mg) and either QD-PLA-PEG-OCH_3 (15 mg, for nontargeted micelles) or QD-PLA-PEG-OCH_3/Mal (15 mg, for targeted micelles) in 2 mL of DMF at room temperature followed by dropwise DI water (10 mL) addition. After 2 h of stirring, the mixture was dialyzed against DI water (MWCO 15 kDa) to remove DMF and free AF. The final product was lyophilized to obtain AF-encapsulated micelles.

Synthesis of 7D12 Nb-Conjugated, AF-Encapsulated QD-PLA-PEG Micelles (i.e., QD-PLA-PEG-OCH_3/7D12 Nb, Abbreviated as QD-PLA-PEG-Nb)

The refolded 7D12 Nbs were conjugated to the surfaces of AF-encapsulated QD-PLA-PEG-OCH_3/Mal micelles by a maleimide–thiol reaction. The feed molar ratio of Nb/micelles was 6:1. Briefly, QD-PLA-PEG-OCH_3/Mal (16.3 mg, 0.023 μmol) was dispersed in 2 mL of 10 mM PBS containing Nbs (0.14 μmol, 2.2 mg). TCEP (0.17 μmol, 0.05 mg) was added to

avoid disulfide bond formation between the Nbs. After being stirred for 4 h at 4 °C, the mixture was centrifuged (10 000 rpm, 4 °C) for 15 min. The pellets were washed twice with 10 mM PBS and redispersed in 10 mM PBS for the following experiments.

Characterization

The chemical structures of all polymer products were analyzed by ^{1}H NMR spectroscopy. The hydrodynamic size and zeta-potential of the micelles were characterized using a Malvern dynamic light scattering (DLS) spectrometer (Zetasizer Nano ZS) at a 90° detection angle. The concentration of the micelles used for the DLS measurement was 0.15 mg/mL. Transmission electron microscopy (TEM, Philips CM200 Ultra Twin) was used to observe the morphology of the dried micelles. TEM samples were prepared by depositing a drop of micelle solution (0.05 mg/mL) with 0.8 wt % phosphotungstic acid onto a carbon-film-coated copper grid (200 mesh) followed by drying. The AF loading level was determined on the basis of its absorbance at 357 nm as measured by a UV–vis spectrometer (Agilent Technologies, Cary 5000 UV–vis–NIR).

In Vitro Drug Release

A 3 mL portion of AF-encapsulated QD-PLA-PEG-Nb micelle solution (1 mg/mL) stored in a dialysis bag (MWCO 15 kDa) was incubated in 27 mL of (1) PBS (pH 7.4), (2) bovine plasma (pH 7.4), or (3) acetate-buffered solution (ABS) (pH 5.3) at 37 °C in a horizontal laboratory shaker (100 rpm). At each time interval, a fixed amount of samples (3 mL) were collected, and an equivalent amount of fresh medium (3 mL) was added. The amount of AF in these samples was measured as detailed above.

Cell Culture

The MDA-MB-468 human TNBC cell line was acquired from ATCC (Manassas, VA). The cells were cultured in 10% fetal bovine serum (FBS)-containing Dulbecco's Modified Eagle Medium (DMEM; Thermo Fisher Scientific, Waltham, MA) in a humidified atmosphere of 37 °C and 5% CO_2. The cell line identity was validated using short tandem repeat profiling in the Pathology Core at UW—Madison.

Cellular Uptake Studies

The effect of 7D12 Nbs on the cellular uptake of the QD-PLA-PEG micelles was studied using both fluorescence microscopy and flow cytometry based on QD fluorescence. For fluorescent imaging, MDA-MB-468 cells (2.5×10^4/well) were seeded in an eight-well Chamber Slide system (Nunc Lab-Tek, Thermo Fisher Scientific, Waltham, MA) overnight. Cells were treated with DMEM + 2% FBS media (i.e., control media), media containing 200 μg/mL Nb-lacking micelles (i.e., nontargeted; NT), media containing 200 μg/mL Nb-conjugated micelles (i.e., targeted; T), or a combination of Nb-conjugated micelles and excessive (2 μM) free Nb (i.e., the competitive binding assay) in duplicate wells per treatment. After the cells were incubated (37 °C, 5% CO_2) for 2 h, they were washed three times with 10 mM PBS, fixed with 4% paraformaldehyde (10 mM PBS, 5 min), and mounted with DAPI-containing ProLong Gold Antifade Mountant (Thermo Fisher Scientific, Waltham, MA). Images were obtained on a fluorescence microscope using the

fluorescence of QDs (excitation wavelength, 488 nm; emission wavelength, 560 nm). For flow cytometry studies, cells (2.0×10^5/well in six-well plates) were treated with DMEM + 2% FBS media (i.e., control), media containing 200 μg/mL micelles without Nb conjugation (i.e., nontargeted), media containing 200 μg/mL Nb-conjugated (i.e., targeted) micelles, or a combination of targeted micelles and excessive (2 μM) free Nb (i.e., the competitive binding assay). Each treatment was performed in triplicate wells. After 2 h of treatment, cells were washed twice with 10 mM PBS (to remove any remaining free micelles in the media), detached from the cell culture plate using 0.25% trypsin (Thermo Fisher Scientific, Waltham, MA), and collected by centrifugation at 125 g for 5 min. The MDA-MB-468 cells were subsequently resuspended in 500 μL of 10 mM PBS after they were washed twice with 10 mM PBS. The fluorescence of the QD (the core of the micelles) was used to quantify cellular uptake. Data were acquired and analyzed using an Accuri C6 flow cytometry system (BD Biosciences, San Jose, CA) and FlowJo software.

Cell Viability Studies Using MTT Assays

The cytotoxicity of the QD-PLA-PEG micelles was studied by *in vitro* MTT assays. MDA-MB-468 cells (5000/well in 96-well plates) were treated with DMEM + 10% FBS media (i.e., control), media containing free AF, media containing AF-encapsulated nontargeted QD-PLA-PEG micelles (AF-NT), media containing AF-encapsulated targeted QD-PLA-PEG micelles (AF-T), or media containing empty (drug free) targeted (Empty T) or nontargeted (Empty NT) QD-PLA-PEG micelles with equivalent AF concentrations. Two equivalent AF concentrations, namely, 0.05 or 0.1 μg/mL, were investigated. Each treatment condition had five replicates. After 24 h of treatment, cells were treated with media containing 0.5 mg/mL MTT and incubated for another 4 h. The MTT-containing medium was aspirated. Next, the purple precipitates were dissolved in 150 μL of DMSO. A GloMax-Multi+ detection system (Promega, Fitchburg, WI) with a reference absorbance at 730 nm was used to measure the absorbance at 560 nm.

In Vivo Biodistribution and Anticancer Efficacy of Micelles

All animal work complied with the procedure approved by the Institutional Animal Care and Use Committee of the University of Wisconsin—Madison. Approximately 1×10^6 MDA-MB-468 cells per site were injected bilaterally into the inguinal mammary fat pads of athymic nude-Foxn1^{nu} mice (Harlan Laboratories, Indianapolis, IN) when they were 5–6 weeks old. Palpable tumors were detected in approximately two months. Five treatments at intervals of 4 days apart were administered retro-orbitally to the mice. Treatment conditions included PBS, free AF, empty Nb-conjugated targeted (Empty T) micelles, and AF-encapsulated QD-PLA-PEG micelles including nontargeted micelles (AF-NT) and targeted micelles (AF-T). The equivalent concentration of AF in each treatment condition was set at 7 mg/kg body weight (BW). *In vivo* drug biodistribution was determined using an *in vivo* imaging system (IVIS) (Waltham, MA). Targeted or nontargeted micelles were injected intravenously in MDA-MB-468 tumor-bearing mice, and images were taken 5 and 24 h postinjection using the fluorescence of the QDs (excitation wavelength, 640 nm; emission wavelength, 740 nm). At each time point, tumor dimensions were determined using an electronic caliper, and the volume was quantified according to a modified ellipsoid formula.[53]

Histological Analysis

The lung, liver, kidney, and spleen tissues from the sacrificed mice were immediately fixed in 10% formalin for 48 h, followed by two washes with 70% ethanol and storage in 70% ethanol. Then, the samples were embedded in paraffin and cut into 5–7 μm thick sections. Hematoxylin and eosin (H&E) staining was performed following standard procedures.[34] Tissues were imaged under a Leica DM 5000B upright microscope, and all data were analyzed by the Leica Application Suite software.

RESULTS AND DISCUSSION

Preparation and Characterization of QD-PLA-PEG-OCH_3/7D12 Nb (i.e., QD-PLA-PEG-Nb) Micelles

The QD-PLA-PEG-Nb micelles were synthesized following Scheme 1. First, InP/ZnS QDs were synthesized using a simple one-pot solvothermal method. The size of the QDs ranged from 3 to 5 nm (Figure S1). The fluorescence emission peak of the QDs upon 640 nm excitation ranged from 500 to 800 nm, with a peak located at 650 nm (Figure S2b). Thereafter, the QDs were surfaced-modified with carboxyl groups for the subsequent conjugation of PLA-PEG-OCH_3 or PLA-PEG-Mal amphiphilic block copolymers, which were synthesized by ring-opening polymerization using CH_3O-PEG-OH and Mal-PEG-OH as macroinitiators, respectively. Their chemical structures were confirmed by ^{1}H NMR. On the basis of the NMR peak intensity ratio between the LA repeat units and the terminal LA at 5.25 and 4.60 ppm, respectively, the number of repeat units in the PLA segments was calculated to be 17. PLA-PEG-OCH_3 and PLA-PEG-Mal were conjugated to the surface of the carboxyl-modified QDs by DCC/DMAP catalyzed esterification. The feeding molar ratio of QD-COOH/PLA-PEG-OCH_3/PLA-PEG-Mal was 1:90:10.

QD-PLA-PEG micelles were dispersed stably in an aqueous solution (Figure S3). Nbs were refolded by dialysis against renaturation buffers with decreasing urea concentrations from 8 M to 0, and selectively conjugated to the distal ends of the PEG arms by a thiol-maleimide reaction in PBS. The feed molar ratio of Nb and micelle was set at 6:1.

The average hydrodynamic diameter of the micelles was 46 nm according to DLS analysis (Figure 1a). The zeta-potential of the micelles was –3.27 mV, indicating that the surfaces of the micelles were nearly neutral. The morphology of the dried micelles was studied by TEM (Figure 1b). The dried micelles had a diameter of about 40 nm.

pH-Sensitive Drug Release Profiles

The AF loading content and AF release profiles of the AF-encapsulated QD-PLA-PEG micelles were determined *in vitro*. The loading content of AF was calculated to be 21.4 wt %. As shown in Figure 2, drug release studies were performed *in vitro* at 37 °C in three different media: (1) PBS (pH 7.4), (2) plasma (pH 7.4), and (3) ABS (pH 5.3). As shown in Figure 2, at pH 5.3, AF release was much faster than that at neutral pH (PBS or plasma). At pH 5.3 (ABS), 36% of the total AF was released after 24 h, 53% after 48 h, and 76% after 120 h. In contrast, at pH 7.4 (PBS) and plasma, 24 h postincubation, only 15% of the AF was released. After 120 h, 21% and 34% of AF was released at pH 7.4 and plasma,

respectively. These results demonstrated the pH-dependent release behavior of AF-encapsulated micelles, which is advantageous for targeted cancer therapy.

Effect of Nanobody Conjugation on the Uptake of QD-PLA-PEG Micelles by MDA-MB-468 TNBC Cells

The effect of anti-EGFR nanobody (7D12) conjugation on the cellular uptake of micelles in an EGFR-overexpressing TNBC cell line was determined using flow cytometry and fluorescent microscopy. The fluorescence of the QDs, which were the cores of the micelles, was used to study the cellular uptake of the micelles. As shown in Figure 3, the cellular uptake of Nb-conjugated (i.e., targeted (T)) micelles was 67-fold higher than that of the Nb-lacking (i.e., nontargeted (NT)) micelles in EGFR-overexpressing MDA-MB-468 cells. Furthermore, the competitive binding assay clearly showed that the cellular uptake of targeted micelles in the presence of free Nbs (Figure 3, denoted as CB) was indistinguishable from that of the nontargeted (NT) micelles. These results demonstrate that the cellular uptake of the QD-PLA-PEG micelles in cancer cells with EGFR overexpression was enhanced by nanobody 7D12 conjugation.

This finding was further confirmed by fluorescent microscopy analyses. As shown in Figure 4, MDA-MB-468 cells treated with targeted micelles showed drastically higher QD fluorescence intensities than the ones treated with either nontargeted micelles or the competitive binding assay.

Effect of Nanobody Conjugation on the Cytotoxicity of AF-Encapsulated QD-PLA-PEG Micelles

The cytotoxicity of the AF-encapsulated, Nb-conjugated micelles against MDA-MB-468 tumor cells was studied using MTT assays. The cytotoxicity of the AF-encapsulated targeted (AF-T) micelles was similar to that of the free AF *in vitro* at the two AF concentrations (i.e., 0.05 and 0.1 μg/mL) investigated (Figure 5). However, AF-encapsulated targeted micelles (AF-T) induced significantly higher cytotoxicity at both concentrations when compared with AF-encapsulated nontargeted ones (AF-NT) (Figure 5). It is worth noting that Empty T micelles also elicited a statistically significant decrease in cell viability ($p = 0.048$ and $p = 0.015$ at AF concentrations of 0.05 and 0.1 μg/mL, respectively). In contrast, treatment of Empty NT micelles did not show a significant reduction in cell viability, thus indicating low cytotoxicity of the QDs. The cytotoxicity of Empty T micelles appears to have been caused by 7D12 Nb's inhibiting ability against EGFR-dependent tumor cell proliferation.[54,55] Overall, the Nb-conjugated and AF-encapsulated QD-PLA-PEG micelles elicited strong cytotoxic effects in EGFR-overexpressed TNBCs.

Effect of Nanobody Conjugation on the Tumor-Targeting Ability of QD-PLA-PEG Micelles

To assess the uptake of nontargeted and targeted QD-PLA-PEG micelles *in vivo*, these micelles were administered intravenously into MDA-MB-468 tumor-bearing mice, and the fluorescence images of the QD cores were recorded (excitation, 640 nm; emission, 740 nm) at 5 and 24 h postinjection (Figure 6a). Significantly stronger fluorescence intensities were shown in mice treated with targeted micelles than those treated with nontargeted micelles at both time points (Figure 6b). The enhanced accumulation of Nb-conjugated micelles in

EGFR-overexpressing tumors ensured that anti-EGFR Nb, 7D12, is effective as a tumor-targeting ligand. Furthermore, the QD core of the micelle can effectively function as an imaging agent *in vivo* for real-time monitoring of QD-PLA-PEG micelle uptake in tumors.

Effect of Nanobody Conjugation on the Antitumor Efficacy of AF-Encapsulated QD-PLA-PEG Micelles in a MDA-MB-468 Orthotopic Xenograft Mouse Model

The antitumor effect of the AF-encapsulated targeted micelles was assessed in an orthotopic xenograft mouse model. Figure 7a shows the workflow of the *in vivo* experimental design. There was no statistical difference among the anticancer effects of the control (i.e., PBS), empty targeted micelles (i.e., Empty T), and free AF groups. In contrast, both AF-encapsulated micelles (targeted (AF-T) and nontargeted (AF-NT)) strongly inhibited tumor growth. We observed that tumors regressed after the fourth injection of AF-encapsulated targeted QD-PLA-PEG micelles and the tumors remained unchanged from day 20 to day 40 when the mice were sacrificed. These data suggest that anti-EGFR Nb conjugation greatly enhanced the anticancer efficacy of the AF-encapsulated micelles *in vivo* (Figure 7b). Therefore, AF-encapsulated Nb-conjugated targeted QD-PLA-PEG micelles may be a viable therapeutic option for the treatment of EGFR-overexpressing TNBC.

CONCLUSIONS

A QD-PLA-PEG micelle conjugated with anti-EGFR nanobody, 7D12, was engineered as a therapeutic agent for EGFR-overexpressing cancers. Because the InP/ZnS QD core of the micelles exhibited stable NIR fluorescence, the localization of the micelles could be monitored through optical imaging *in vitro* and *in vivo. In vitro* studies demonstrated that anti-EGFR Nb conjugation to the surfaces of the micelles facilitated cellular uptake and increased cytotoxicity of the AF-encapsulated micelles in EGFR-overexpressing MDA-MB-468 cells. Consequently, in an MDA-MB-468 breast cancer xenograft mouse model, the Nb-conjugated QD-PLA-PEG micelles exhibited a much better tumor-targeting ability over the nontargeted ones. For the *in vivo* anticancer studies, neither the free drug nor the empty targeted micelle treatment groups showed any anticancer effects. In contrast, the AF-encapsulated nontargeted QD-PLA-PEG micelles significantly inhibited the growth of TNBC tumors, while the AF-encapsulated Nb-conjugated QD-PLA-PEG micelles effectively induced tumor regression. At the AF dosage used for the treatments, systemic toxicity was not observed with the AF-encapsulated Nb-conjugated QD-PLA-PEG micelles judging by the body weight measurements and organ histological analyses. These findings suggest that the Nb-conjugated QD-PLA-PEG micelles could potentially serve as a targeted theranostic option for EGFR-overexpressing cancers, including TNBC.

The body weights of the mice were monitored through treatment. The body weights of the mice remained steady during treatment, and no difference was observed between the treatment groups and the control group (Figure 8a). Major organ sections (lung, liver, kidney, and spleen) were stained with H&E and pathologically assessed for each treatment arm including the control, free AF, Empty T, AF-T, and AF-NT. As shown in Figure 8b, the morphologies of the respective tissues were normal, and no acute or chronic inflammation, or apoptotic or necrotic regions, was found in any of the five groups of animals studied,

suggesting that no adverse effects were caused by AF-encapsulated Nb-conjugated targeted QD-PLA-PEG micelles in the orthotopic MDA-MB-468 TNBC xenograft mouse model.

Supplementary Material

Refer to Web version on PubMed Central for supplementary material.

Acknowledgments

Financial support from the NIH (1K25CA166178 to S.G. and R21CA196653 to W.X. and S.G.) is greatly appreciated. The project was also partially supported by the NIH/NCI P30CA014520 UW Cancer Center support grant.

References

1. Torchilin VP. Multifunctional Nanocarriers. Adv Drug Delivery Rev. 2012; 64:302–315.
2. Xiao Y, Hong H, Javadi A, Engle JW, Xu W, Yang Y, Zhang Y, Barnhart TE, Cai W, Gong S. Multifunctional Unimolecular Micelles for Cancer-targeted Drug Delivery and Positron Emission Tomography Imaging. Biomaterials. 2012; 33:3071–3082. [PubMed: 22281424]
3. Guo J, Hong H, Chen G, Shi S, Nayak TR, Theuer CP, Barnhart TE, Cai W, Gong S. Theranostic Unimolecular Micelles Based on Brush-shaped Amphiphilic Block Copolymers for Tumor-targeted Drug Delivery and Positron Emission Tomography Imaging. ACS Appl Mater Interfaces. 2014; 6:21769–21779. [PubMed: 24628452]
4. Chen G, Jaskula-Sztul R, Harrison A, Dammalapati A, Xu W, Cheng Y, Chen H, Gong S. Ke108-Conjugated Unimolecular Micelles Loaded with a Novel HDAC Inhibitor Thailandepsin-A for Targeted Neuroendocrine Cancer Therapy. Biomaterials. 2016; 97:22–33. [PubMed: 27156249]
5. Yang X, Hong H, Grailer JJ, Rowland IJ, Javadi A, Hurley SA, Xiao Y, Yang Y, Zhang Y, Nickles RJ, Cai W, Steeber DA, Gong S. cRGD-functionalized, Dox-conjugated, and 64Cu-labeled Superparamagnetic Iron Oxide Nanoparticles for Targeted Anticancer Drug Delivery and PET/MR Imaging. Bio-materials. 2011; 32:4151–4160.
6. Xu W, Siddiqui IA, Nihal M, Pilla S, Rosenthal K, Mukhtar H, Gong S. Aptamer-conjugated and Doxorubicin-Loaded Unimolecular Micelles for Targeted Therapy of Prostate Cancer. Biomaterials. 2013; 34:5244–5253. [PubMed: 23582862]
7. Sun W, Hu Q, Ji W, Wright G, Gu Z. Leveraging Physiology for Precision Drug Delivery. Physiol Rev. 2017; 97:189–225.
8. Lu Y, Aimetti AA, Langer R, Gu Z. Bioresponsive Materials. Nat Rev Mater. 2016; 2:16075.
9. Medintz IL, Uyeda HT, Goldman ER, Mattoussi H. Quantum Dot Bioconjugates for Imaging, Labelling and Sensing. Nat Mater. 2005; 4:435–446. [PubMed: 15928695]
10. Resch-Genger U, Grabolle M, Cavaliere-Jaricot S, Nitschke R, Nann T. Quantum Dots Versus Organic Dyes as Fluorescent Labels. Nat Methods. 2008; 5(9):763–775. [PubMed: 18756197]
11. Escobedo JO, Rusin O, Lim S, Strongin RM. NIR Dyes for Bioimaging Applications. Curr Opin Chem Biol. 2010; 14:64–70. [PubMed: 19926332]
12. Guo Z, Park S, Yoon J, Shin I. Recent Progress in the Development of Near-infrared Fluorescent Probes for Bioimaging Applications. Chem Soc Rev. 2014; 43:16–29. [PubMed: 24052190]
13. Larson DR, Zipfel WR, Williams RM, Clark SW, Bruchez MP, Wise FW, Webb WW. Water-soluble Quantum Dots for Multiphoton Fluorescence Imaging In Vivo. Science. 2003; 300:1434–1436. [PubMed: 12775841]
14. Michalet X, Pinaud FF, Bentolila LA, Tsay JM, Doose S, Li JJ, Sundaresan G, Wu AM, Gambhir SS, Weiss S. Quantum Dots for Live Cells, In Vivo Imaging, and Diagnostics. Science. 2005; 307:538–544. [PubMed: 15681376]
15. Gao X, Yang L, Petros JA, Marshall FF, Simons JW, Nie S. In Vivo Molecular and Cellular Imaging with Quantum Dots. Curr Opin Biotechnol. 2005; 16:63–72. [PubMed: 15722017]

16. Chibli H, Carlini L, Park S, Dimitrijevic NM, Nadeau JL. Cytotoxicity of Inp/Zns Quantum Dots Related to Reactive Oxygen Species Generation. Nanoscale. 2011; 3:2552–2559. [PubMed: 21509403]
17. Brunetti V, Chibli H, Fiammengo R, Galeone A, Malvindi MA, Vecchio G, Cingolani R, Nadeau JL, Pompa PP. Inp/Zns as a Safer Alternative to Cdse/Zns Core/Shell Quantum Dots: In Vitro and In Vivo Toxicity Assessment. Nanoscale. 2013; 5:307–317. [PubMed: 23165345]
18. Bharali DJ, Lucey DW, Jayakumar H, Pudavar HE, Prasad PN. Folate-Receptor-Mediated Delivery of Inp Quantum Dots for Bioimaging Using Confocal and Two-photon Microscopy. J Am Chem Soc. 2005; 127:11364–11371. [PubMed: 16089466]
19. Yang X, Zhao D, Leck KS, Tan ST, Tang YX, Zhao J, Demir HV, Sun XW. Full Visible Range Covering Inp/Zns Nanocrystals with High Photometric Performance and Their Application to White Quantum Dot Light-emitting Diodes. Adv Mater. 2012; 24:4180–4185. [PubMed: 22544765]
20. Deng C, Jiang Y, Cheng R, Meng F, Zhong Z. Biodegradable Polymeric Micelles for Targeted and Controlled Anticancer Drug Delivery: Promises, Progress and Prospects. Nano Today. 2012; 7:467–480.
21. Ge Z, Liu S. Functional Block Copolymer Assemblies Responsive to Tumor and Intracellular Microenvironments for Site-specific Drug Delivery and Enhanced Imaging Performance. Chem Soc Rev. 2013; 42:7289–7325. [PubMed: 23549663]
22. Prabaharan M, Grailer JJ, Pilla S, Steeber DA, Gong S. Folate-conjugated Amphiphilic Hyperbranched Block Copolymers Based on Boltorn® H40, Poly (L-lactide) and Poly(ethylene glycol) for Tumor-targeted Drug Delivery. Biomaterials. 2009; 30:3009–3019. [PubMed: 19250665]
23. Guo J, Hong H, Chen G, Shi S, Zheng Q, Zhang Y, Theuer CP, Barnhart TE, Cai W, Gong S. Image-guided and Tumor-targeted Drug Delivery with Radiolabeled Unimolecular Micelles. Biomaterials. 2013; 34:8323–8332. [PubMed: 23932288]
24. Cao W, Zhou J, Mann A, Wang Y, Zhu L. Folate-functionalized Unimolecular Micelles Based on a Degradable Amphiphilic Dendrimer-like Star Polymer for Cancer Cell-targeted Drug Delivery. Biomacromolecules. 2011; 12:2697–2707. [PubMed: 21619062]
25. Prabaharan M, Grailer JJ, Pilla S, Steeber DA, Gong S. Gold Nanoparticles with a Monolayer of Doxorubicin-conjugated Amphiphilic Block Copolymer for Tumor-targeted Drug Delivery. Biomaterials. 2009; 30:6065–6075. [PubMed: 19674777]
26. Chen G, Jaskula-Sztul R, Esquibel CR, Lou I, Zheng Q, Dammalapati A, Harrison A, Eliceiri KW, Tang W, Chen H, Gong S. Neuroendocrine Tumor-targeted Upconversion Nano-particle-based Micelles for Simultaneous NIR-controlled Combination Chemotherapy and Photodynamic Therapy, and Fluorescence Imaging. Adv Funct Mater. 2017; 27:1604671. [PubMed: 28989337]
27. Nicholson RI, Gee JMW, Harper ME. EGFR and Cancer Prognosis. Eur J Cancer. 2001; 37(Supplement 4):9–15. [PubMed: 11165124]
28. Verbeek BS, Adriaansen-Slot SS, Vroom TM, Beckers T, Rijksen G. Overexpression of EGFR and c-erbB2 Causes Enhanced Cell Migration in Human Breast Cancer Cells and NIH3T3 Fibroblasts. FEBS Lett. 1998; 425:145–150. [PubMed: 9541025]
29. Normanno N, De Luca A, Bianco C, Strizzi L, Mancino M, Maiello MR, Carotenuto A, De Feo G, Caponigro F, Salomon DS. Epidermal Growth Factor Receptor (EGFR) Signaling in Cancer. Gene. 2006; 366:2–16. [PubMed: 16377102]
30. Erjala K, Sundvall M, Junttila TT, Zhang N, Savisalo M, Mali P, Kulmala J, Pulkkinen J, Grenman R, Elenius K. Signaling Via ErbB2 and erbB3 Associates with Resistance and Epidermal Growth Factor Receptor (EGFR) Amplification with Sensitivity to EGFR Inhibitor Gefitinib in Head and Neck Squamous Cell Carcinoma Cells. Clin Cancer Res. 2006; 12:4103–4111. [PubMed: 16818711]
31. Cappuzzo F, Hirsch FR, Rossi E, Bartolini S, Ceresoli GL, Bemis L, Haney J, Witta S, Danenberg K, Domenichini I, et al. Epidermal Growth Factor Receptor Gene and Protein and Gefitinib Sensitivity in Non-small-cell Lung Cancer. J Natl Cancer Inst. 2005; 97:643–655. [PubMed: 15870435]

32. Spano JP, Lagorce C, Atlan D, Milano G, Domont J, Benamouzig R, Attar A, Benichou J, Martin A, Morere JF. Impact of EGFR Expression on Colorectal Cancer Patient Prognosis and Survival. Ann Oncol. 2005; 16:102–108. [PubMed: 15598946]
33. Bardeesy N, DePinho RA. Pancreatic Cancer Biology and Genetics. Nat Rev Cancer. 2002; 2:897–909. [PubMed: 12459728]
34. Brinkman AM, Chen G, Wang Y, Hedman CJ, Sherer NM, Havighurst TC, Gong S, Xu W. Aminoflavone-loaded EGFR-targeted Unimolecular Micelle Nanoparticles Exhibit Anti-cancer Effects in Triple Negative Breast Cancer. Biomaterials. 2016; 101:20–31. [PubMed: 27267625]
35. Gumuskaya B, Alper M, Hucumenoglu S, Altundag K, Uner A, Guler G. EGFR Expression and Gene Copy Number in Triple-negative Breast Carcinoma. Cancer Genet Cytogenet. 2010; 203:222–229. [PubMed: 21156237]
36. Reis-Filho JS, Pinheiro C, Lambros MBK, Milanezi F, Carvalho S, Savage K, Simpson PT, Jones C, Swift S, Mackay A, et al. EGFR Amplification and Lack of Activating Mutations in Metaplastic Breast Carcinomas. J Pathol. 2006; 209:445–453. [PubMed: 16739104]
37. El-Sayed IH, Huang X, El-Sayed MA. Surface Plasmon Resonance Scattering and Absorption of Anti-EGFR Antibody Conjugated Gold Nanoparticles in Cancer Diagnostics: Applications in Oral Cancer. Nano Lett. 2005; 5(5):829–834. [PubMed: 15884879]
38. El-Sayed IH, Huang X, El-Sayed MA. Selective Laser Photo-thermal Therapy of Epithelial Carcinoma Using Anti-EGFR Antibody Conjugated Gold Nanoparticles. Cancer Lett. 2006; 239:129–135. [PubMed: 16198049]
39. Yang L, Mao H, Wang YA, Cao Z, Peng X, Wang X, Duan H, Ni C, Yuan Q, Adams G, et al. Single Chain Epidermal Growth Factor Receptor Antibody Conjugated Nanoparticles for in Vivo Tumor Targeting and Imaging. Small. 2009; 5:235–243. [PubMed: 19089838]
40. Altintas I, Kok RJ, Schiffelers RM. Targeting Epidermal Growth Factor Receptor in Tumors: From Conventional Monoclonal Antibodies via Heavy Chain-Only Antibodies to Nanobodies. Eur J Pharm Sci. 2012; 45:399–407. [PubMed: 22064454]
41. Oliveira S, Heukers R, Sornkom J, Kok RJ, van Bergen en Henegouwen PM. Targeting Tumors with Nanobodies for Cancer Imaging and Therapy. J Controlled Release. 2013; 172:607–617.
42. Schmitz KR, Bagchi A, Roovers RC, van Bergen en Henegouwen PM, Ferguson KM. Structural Evaluation of EGFR Inhibition Mechanisms for Nanobodies/VHH Domains. Structure. 2013; 21:1214–1224. [PubMed: 23791944]
43. Kijanka M, Dorresteijn B, Oliveira S, van Bergen en Henegouwen PM. Nanobody-based Cancer Therapy of Solid Tumors. Nanomedicine. 2015; 10:161–174. [PubMed: 25597775]
44. Hassanzadeh-Ghassabeh G, Devoogdt N, De Pauw P, Vincke C, Muyldermans S. Nanobodies and Their Potential Applications. Nanomedicine. 2013; 8:1013–1026. [PubMed: 23730699]
45. Oliveira S, Schiffelers RM, van der Veeken J, van der Meel R, Vongpromek R, van Bergen en Henegouwen PM, Storm G, Roovers RC. Downregulation of EGFR by a Novel Multivalent Nanobody-Liposome Platform. J Controlled Release. 2010; 145:165–175.
46. Van de Broek B, Devoogdt N, D'Hollander A, Gijs HL, Jans K, Lagae L, Muyldermans S, Maes G, Borghs G. Specific Cell Targeting with Nanobody Conjugated Branched Gold Nano-particles for Photothermal Therapy. ACS Nano. 2011; 5:4319–4328. [PubMed: 21609027]
47. D'Hollander A, Jans H, Velde GV, Verstraete C, Massa S, Devoogdt N, Stakenborg T, Muyldermans S, Lagae L, Himmelreich U. Limiting the Protein Corona: A Successful Strategy for In Vivo Active Targeting of Anti-HER2 Nanobody-functionalized Nanostars. Biomaterials. 2017; 123:15–23. [PubMed: 28152380]
48. Sukhanova A, Even-Desrumeaux K, Kisserli A, Tabary T, Reveil B, Millot J-M, Chames P, Baty D, Artemyev M, Oleinikov V, et al. Oriented Conjugates of Single-domain Antibodies and Quantum Dots: Toward a New Generation of Ultrasmall Diagnostic Nanoprobes. Nanomedicine (N Y, NY, U S). 2012; 8:516–525.
49. Talelli M, Rijcken CJF, Oliveira S, van der Meel R, van Bergen en Henegouwen PM, Lammers T, van Nostrum CF, Storm G, Hennink WE. "Reprint of" Nanobody-shell Functionalized Thermosensitive Core-crosslinked Polymeric Micelles for Active Drug Targeting. J Controlled Release. 2011; 153:93–102.

50. Zarschler K, Prapainop K, Mahon E, Rocks L, Bramini M, Kelly PM, Stephan H, Dawson KA. Diagnostic Nanoparticle Targeting of the EGFR-receptor in Complex Biological Conditions Using Single-domain Antibodies. Nanoscale. 2014; 6:6046–6056. [PubMed: 24777583]

51. Akama T, Shida Y, Sugaya T, Ishida H, Gomi K, Kasai M. Novel 5-Aminoflavone Derivatives as Specific Antitumor Agents in Breast Cancer. J Med Chem. 1996; 39:3461–3469. [PubMed: 8784443]

52. Li L, Reiss P. One-pot Synthesis of Highly Luminescent InP/ZnS Nanocrystals without Precursor Injection. J Am Chem Soc. 2008; 130:11588–11589. [PubMed: 18686956]

53. Tomayko MM, Reynolds CP. Determination of Subcutaneous Tumor Size in Athymic (Nude) Mice. Cancer Chemother Pharmacol. 1989; 24:148–154. [PubMed: 2544306]

54. Roovers RC, Vosjan MJWD, Laeremans T, el Khoulati R, de Bruin RCG, Ferguson KM, Verkleij AJ, van Dongen GAMS, van Bergen en Henegouwen PM. A Biparatopic Anti-EGFR Nanobody Efficiently Inhibits Solid Tumour Growth. Int J Cancer. 2011; 129:2013–2024. [PubMed: 21520037]

55. Ding L, Tian C, Feng S, Fida G, Zhang C, Ma Y, Ai G, Achilefu S, Gu Y. Small Sized EGFR1 and HER2 Specific Bifunctional Antibody for Targeted Cancer Therapy. Theranostics. 2015; 5:378–398. [PubMed: 25699098]

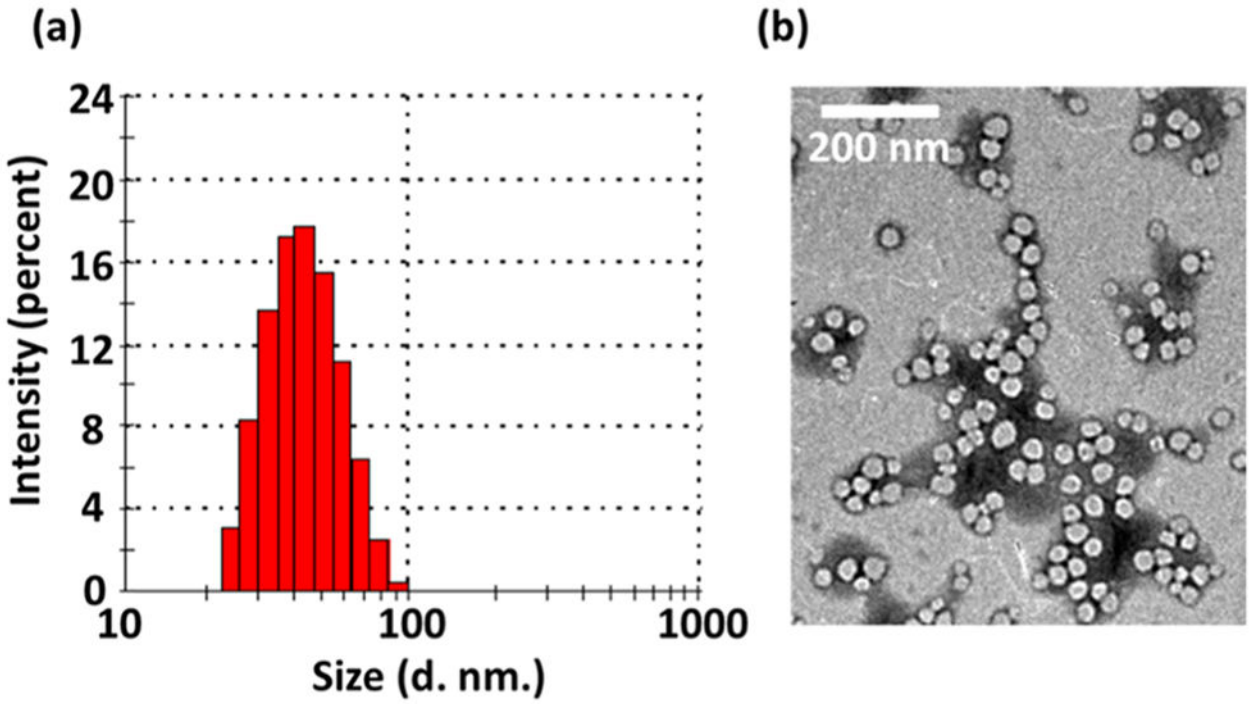

Figure 1.
(a) DLS histogram and (b) TEM image of the QD-PLA-PEG-Nb micelles.

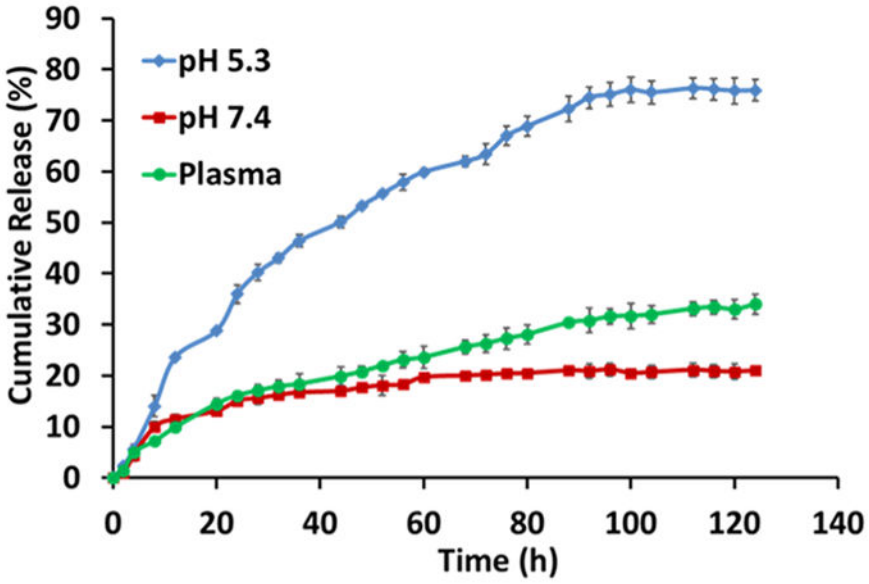

Figure 2.

In vitro cumulative AF release profiles of the AF-encapsulated QD-PLA-PEG micelles measured in ABS (pH 5.3), PBS (pH 7.4), and plasma (pH 7.4).

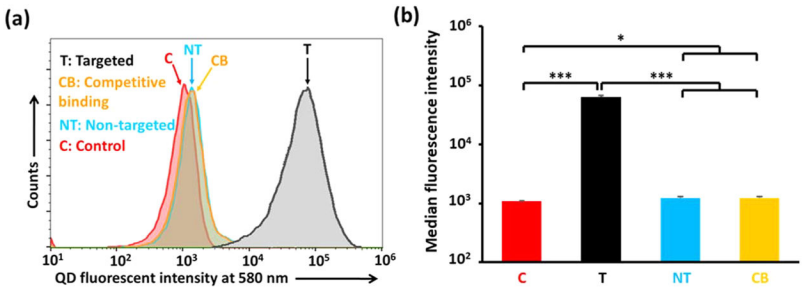

Figure 3.

(a) Cellular uptake studies and (b) median fluorescence intensity analysis of micelles using flow cytometry. The MDA-MB-468 TNBC cells were treated with medium (control), Nb-conjugated (i.e., targeted (T)) QD-PLA-PEG micelles, Nb-lacking (i.e., nontargeted (NT)) QD-PLA-PEG micelles, or a combination of targeted micelles and free Nbs (i.e., the competitive binding assay (CB)). * indicates $p < 0.05$; *** indicates $p < 0.001$.

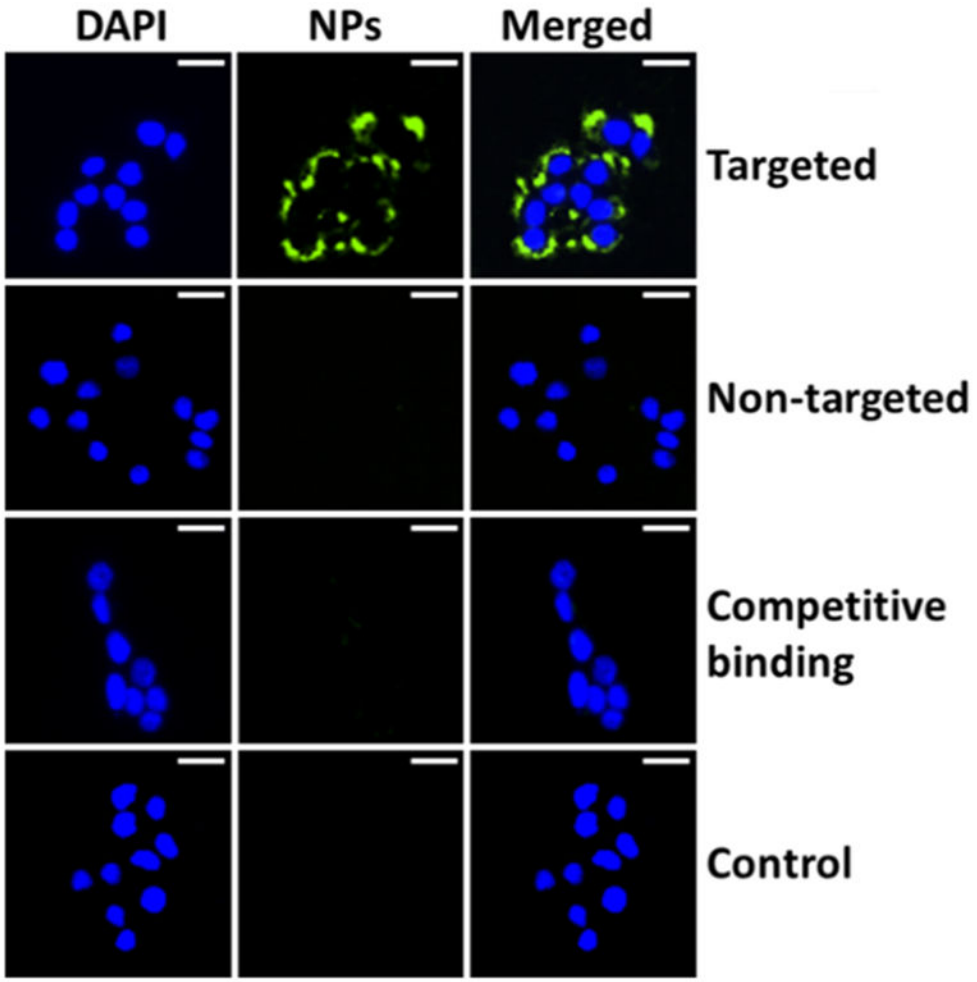

Figure 4.

Cellular uptake studies of QD-PLA-PEG micelles using fluorescence microscopy. Cells were treated with medium (control) or targeted or nontargeted micelles, as well as a combination of targeted micelles and free Nbs (i.e., the competitive binding assay) for 2 h. Scale bar: 25 μm.

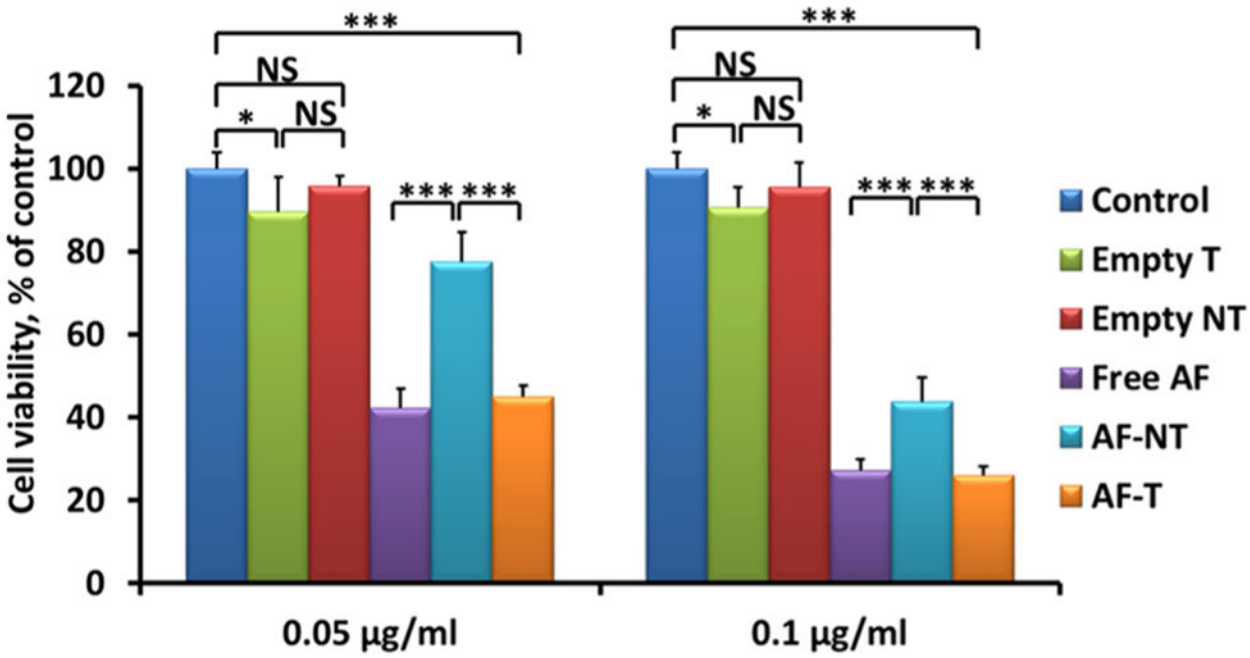

Figure 5.

Cytotoxicity of free AF, empty micelles (Empty NT and Empty T), and AF-encapsulated nontargeted (AF-NT) and targeted (AF-T) QD-PLA-PEG micelles in MDA-MB-468 cells after 24 h incubation at two AF concentrations (0.05 and 0.1 μg/mL). NS: not significant. * indicates $p < 0.05$; *** indicates $p < 0.001$.

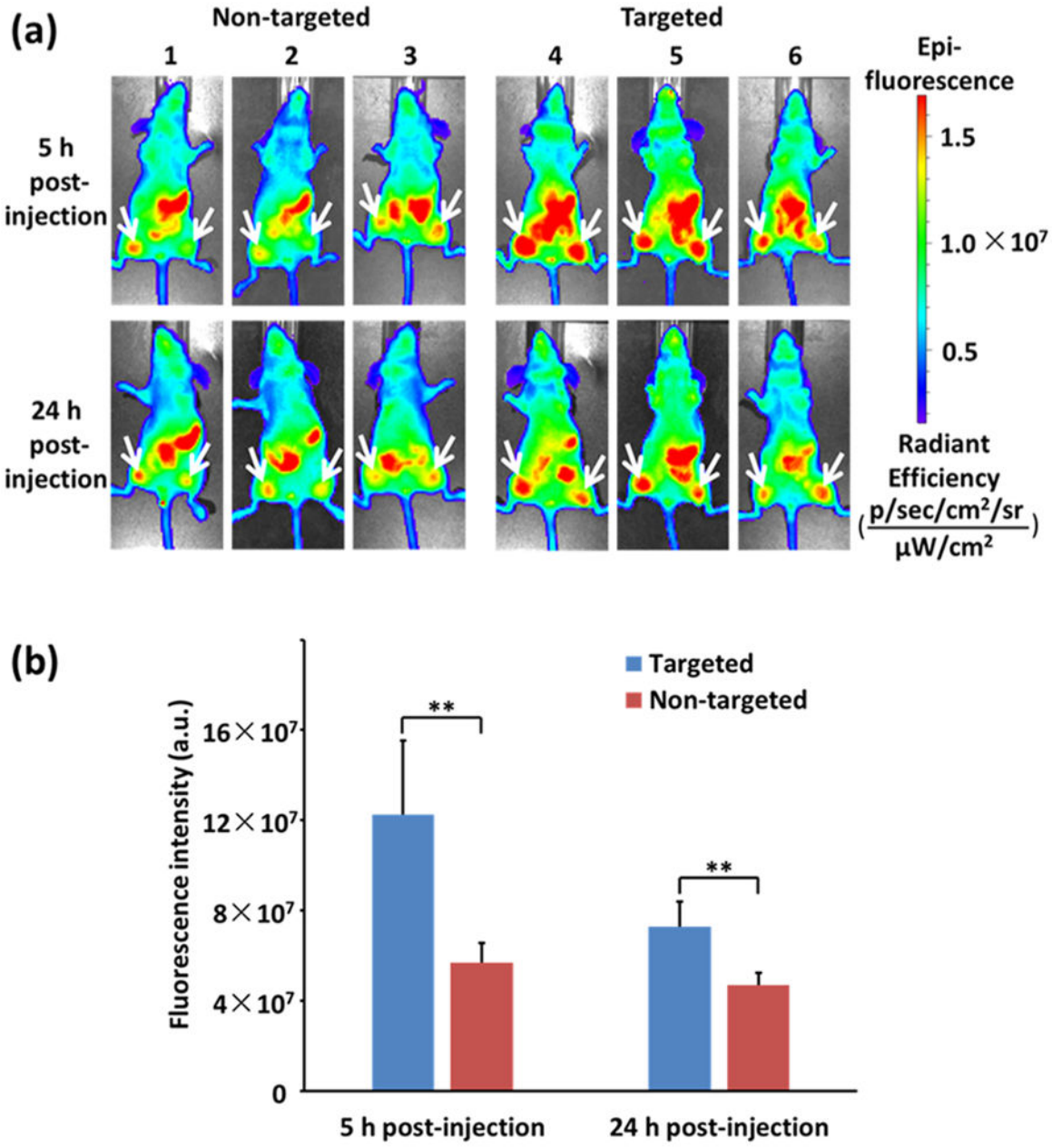

Figure 6.

(a) Fluorescence images of MDA-MB-468 tumors in mice treated with nontargeted (mice 1, 2, and 3) and targeted QD-PLA-PEG micelles (mice 4, 5, and 6). White arrows indicate tumor sites. (b) Fluorescence intensity analysis of the QD-PLA-PEG micelles (targeted and nontargeted) at the MDA-MB-468 tumor sites ($n = 6$) in mice. ** indicates $p < 0.01$.

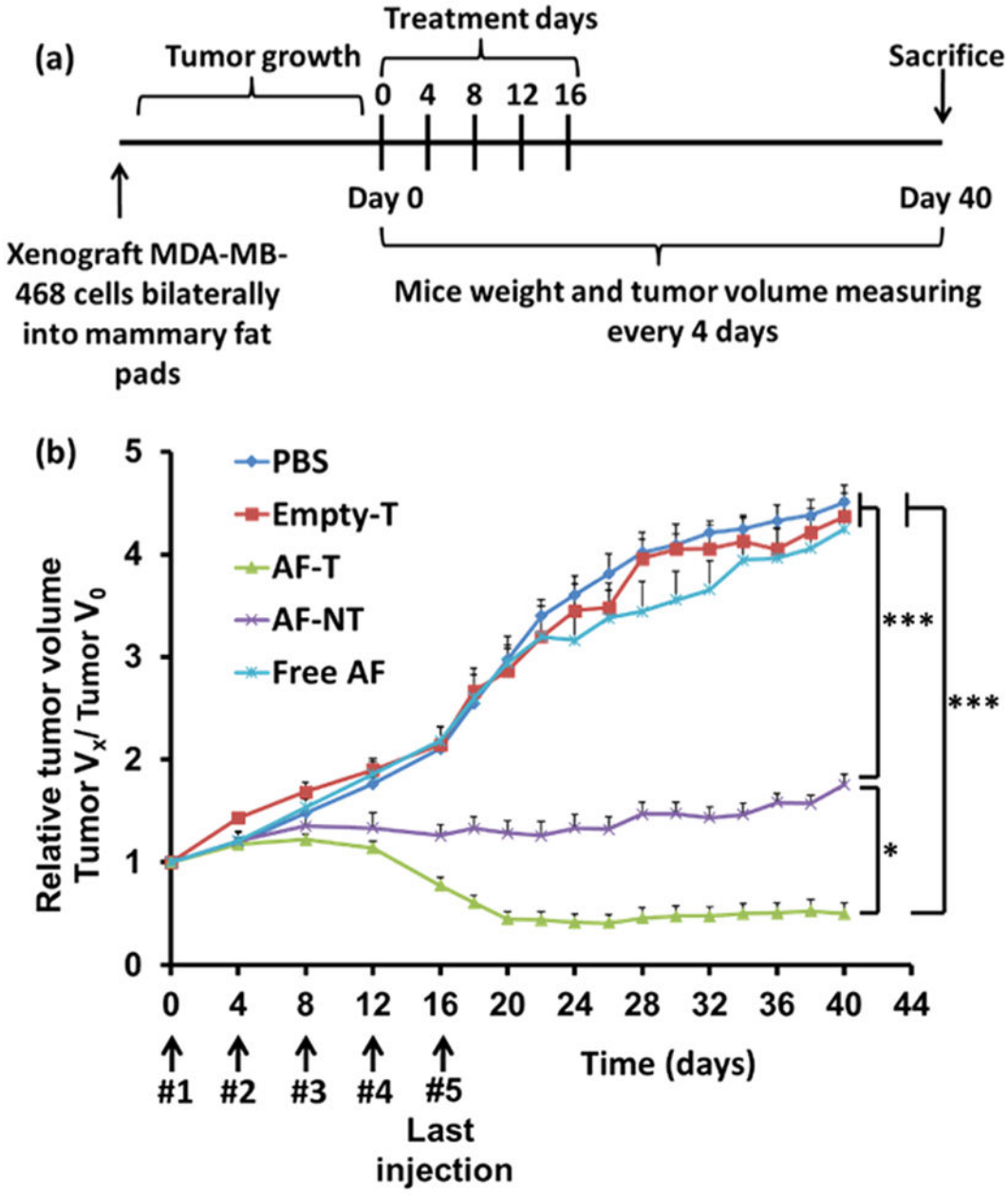

Figure 7.

(a) Timeline for the creation of the orthotopic MDA-MB-468 breast cancer xenograft mouse model and the treatment schedule. Mice were separated into five groups and treated with PBS, free AF, empty targeted micelles (Empty T), or AF-encapsulated QD-PLA-PEG-Nb targeted micelles (AF-T) or QD-PLA-PEG nontargeted micelles (AF-NT)). After the last injection, the mice were kept for 4 weeks. The tumor volumes ($n = 6$) were measured every 4 days. (b) Normalized tumor volume (V_X/V_0) as a function of the treatment time. AF-encapsulated targeted (AF-T) micelles were found to effectively lead to tumor regression. * indicates $p < 0.05$ between AF-T and AF-NT at or after Day 16. *** indicates $p < 0.001$ between AF-T and free AF, and between AF-NT and free AF at or after Day 16.

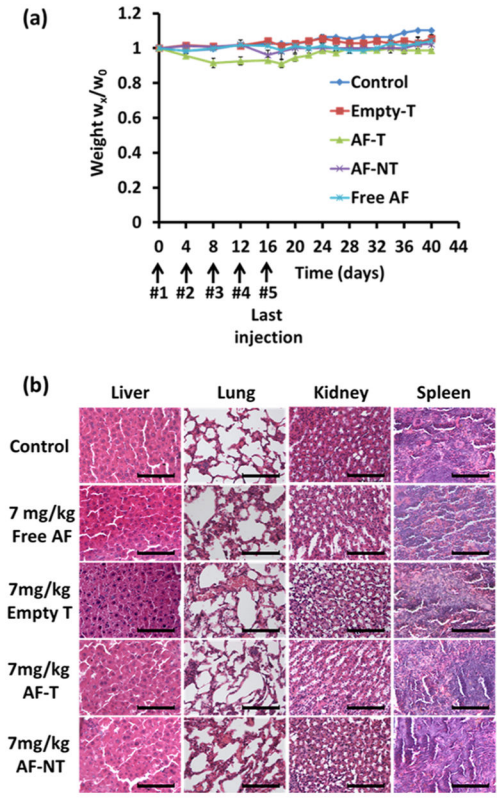

Figure 8.

(a) Body weights of the mice during the course of treatment. (b) Histological analyses (H&E staining) for different organs excised from the orthotopic MDA-MB-468 breast cancer xenograft mice administrated with PBS, free drug, empty targeted (Empty T), and AF-encapsulated targeted (AF-T) or nontargeted (AF-NT) QD-PLA-PEG micelles. For all treatment arms, the equivalent AF concentration was maintained to be the same (i.e., 7 mg/kg). None of the collected organs showed acute or chronic inflammation, or apoptotic or necrotic regions. Scale bar = 100 μm.

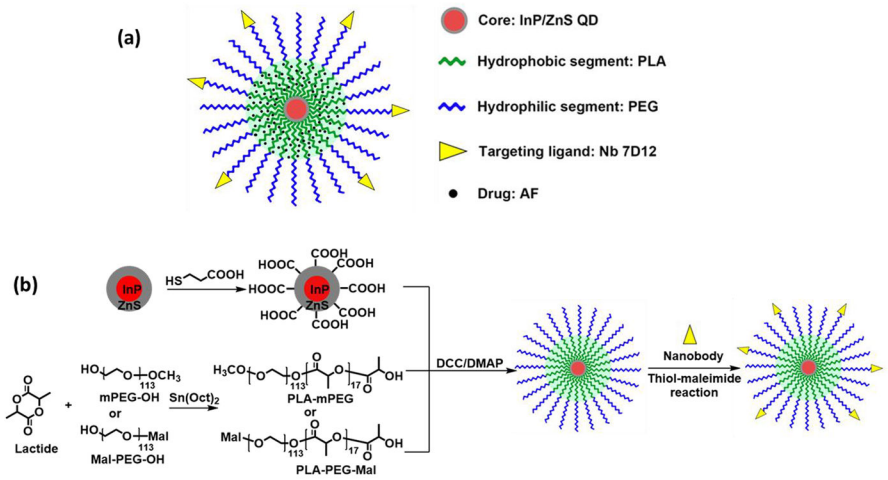

Scheme 1.

(a) Schematic Illustration of the QD-PLA-PEG Micelles Conjugated with 7D12 Nb and (b) Synthesis Scheme for the QD-PLA-PEG-Nb